RESEARCH ARTICLE | JULY 10 2024

Spin-torque ferromagnetic resonance based on current-induced impedance

Yuta Kobayashi ; Tomoya Itoh; Ryusuke Hisatomi ; Takahiro Moriyama ; Yoichi Shiota ; Xin Fan ; Teruo Ono

Appl. Phys. Lett. 125, 022405 (2024)
https://doi.org/10.1063/5.0222114
CHORUS

Applied Physics Letters ARTICLE pubs.aip.org/aip/apl

Spin-torque ferromagnetic resonance based on current-induced impedance

Cite as: Appl. Phys. Lett. **125**, 022405 (2024); doi: 10.1063/5.0222114
Submitted: 5 June 2024 · Accepted: 21 June 2024 ·
Published Online: 10 July 2024

View Online Export Citation CrossMark

Yuta Kobayashi,[1] Tomoya Itoh,[1] Ryusuke Hisatomi,[1,2,3] Takahiro Moriyama,[2,3,4] Yoichi Shiota,[1,2,a)] Xin Fan,[5,a)] and Teruo Ono[1,2]

AFFILIATIONS

[1]Institute for Chemical Research, Kyoto University, Gokasho, Uji, Kyoto 611-0011, Japan
[2]Center for Spintronics Research Network, Kyoto University, Uji, Kyoto 611-0011, Japan
[3]PRESTO, Japan Science and Technology Agency, Kawaguchi, Saitama 322-0012, Japan
[4]Department of Materials Physics, Nagoya University, Nagoya 464-8603, Japan
[5]Department of Physics and Astronomy, University of Denver, Denver 80210, USA

[a)]**Authors to whom correspondence should be addressed:** shiota-y@scl.kyoto-u.ac.jp and xin.fan@du.edu

ABSTRACT

Spin-torque ferromagnetic resonance (ST-FMR) has been widely used for measuring damping-like spin–orbit torques in magnetic bilayers. Typically, the ratio between the damping-like and field-like spin–orbit torques are extrapolated based on the ferromagnetic resonance line shapes. However, when the field-like spin–orbit torque is unknown, the line shape analysis may lead to errors in extrapolating the damping-like spin–orbit torque. Here, we propose a modified version of the ST-FMR that allows extrapolation of both damping-like and field-like torques independently. By introducing an alternating current to the sample, the RF impedance is modulated, allowing detection via the reflected microwave. We show that the extrapolated field-like and damping-like torques in Py/Pt samples are consistent with the technique measuring current-induced linewidth and resonance field change but have much better signal-to-noise ratio. Our proposed method paves a way for more accurate measurement of spin–orbit torques.

Over the past decade, there has been significant interest in studying current-induced spin–orbit torques in magnetic multilayers, primarily due to their potential applications in memory devices.[1–4] Among the various techniques available, spin-torque ferromagnetic resonance (ST-FMR) has emerged as a popular and powerful tool for quantifying spin–orbit torques, owing to its simplicity and high sensitivity.[5,6] The versatility of this technique has facilitated the exploration of new physics, including the orbital Hall effect,[7,8] and has driven the search for materials with efficient spin–orbit torque generation.[9–24]

However, conventional ST-FMR has certain limitations. It relies on fitting symmetric and antisymmetric Lorentzian curves, providing only a ratio between damping-like and field-like torques. In general, field-like torque involves contributions from both Oersted field and field-like spin–orbit torque. Extrapolating the damping-like spin–orbit torque requires making specific assumptions of the field-like torque. For instance, the field-like torque is sometimes assumed to arise solely from the Oersted field,[5] or to have the spin–orbit component that scales inversely with ferromagnet thickness.[25–27] These assumptions may hold true in certain systems, particularly when the ferromagnet is relatively thick. However, in thin ferromagnetic films, the field-like spin–orbit torque can be comparable to or even greater than the Oersted field.[28–30] Experimental studies have also suggested that the field-like spin–orbit torques may have a more sophisticated ferromagnet-thickness dependence.[31,32] While RF current calibration based on microwave reflection has been proposed,[10,33] its limited adoption could be attributed to the challenge of accounting for all impedance mismatches in the microwave circuit.

In this manuscript, we propose and demonstrate a modified ST-FMR measurement technique that addresses these limitations. We introduce an additional low-frequency electric current and measure the resulting RF impedance change. This modified approach not only offers a comparable signal-to-noise ratio to the conventional ST-FMR technique, but also enables more accurate extrapolation of spin–orbit torques.

The principle of current-induced impedance can be understood from the inset of Fig. 1. When a RF current I_{RF} and a low-frequency alternating current I_{AC} are simultaneously applied to a magnetic multilayer, both currents shall induce damping-like and field-like torques. We denote the damping-like torque coefficient $\beta_{DL} = h_{DL} \cdot w/I$ and

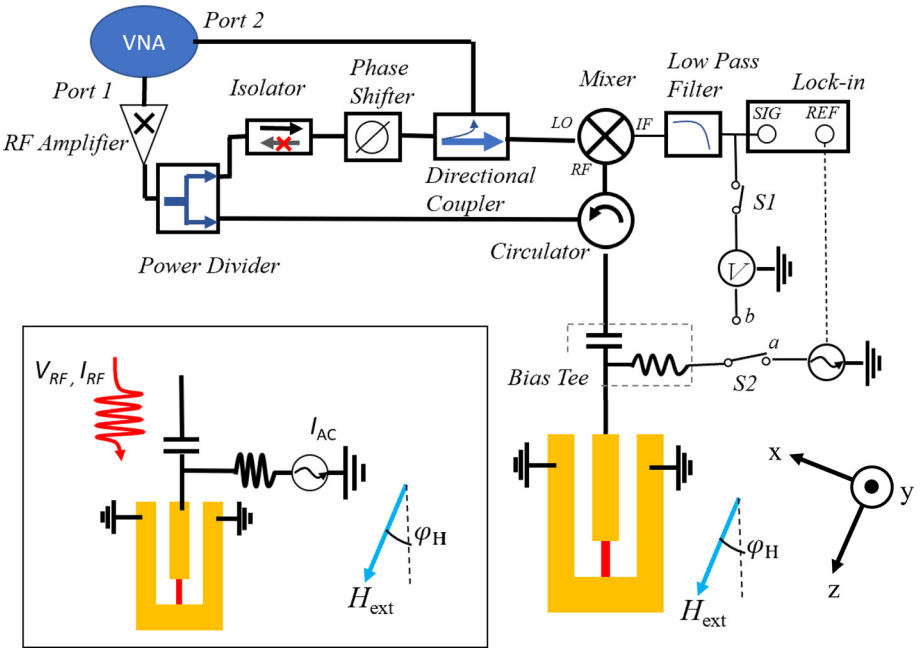

FIG. 1. Schematics of the CIZ-ST-FMR setup. Here, the small red stripe represents the patterned magnetic film under study, and orange stripes represent the coplanar waveguide. The sample is placed above a rotatable projective magnet that provides in-plane magnetic field in an arbitrary direction. The sample is contacted by GSG-type pico probe, which is connected to the microwave circuit as shown. Here, VNA is short for vector network analyzer. The inset shows a simplified circuit to highlight the working principle of the CIZ-ST-FMR setup.

field-like torque coefficient $\beta_{FL} = h_{FL} \cdot w/I$, where w is the width of the device, I is the applied current, h_{DL} is the equivalent field due to damping-like torque, and h_{FL} is the total in-plane current-induced field including contributions from Oersted field and field-like spin–orbit torque. β_{DL} and β_{FL} are unitless experimental measurables. (see section 3 in the supplementary material for their relations to the effective spin Hall angles).

Both IRF and IAC induce in-plane magnetization perturbation,

$$\Delta m = \frac{\beta_{FL}\chi^{AC} I_{AC} + \beta_{FL}\chi_{xx}^{RF} I_{RF} + \beta_{DL}\chi_{xy}^{RF} I_{RF}}{w \cdot M_s} \cos\varphi_H. \quad (1)$$

Here, φ_H is the angle between applied current and equilibrium magnetization. χ^{AC} is the low-frequency magnetic susceptibility, which is a real number. χ_{xx}^{RF} and χ_{xy}^{RF} are the diagonal and off diagonal terms of the RF magnetic susceptibility tensor, respectively, which are complex numbers capturing ferromagnetic resonance.

In-plane magnetization perturbation leads to anisotropic magnetoresistance change ΔR, which couples with the applied AC and RF currents, giving rise to various voltage terms (see supplementary material 1). Among the voltage terms, there arises a term corresponding to the AC-induced RF voltage,

$$\Delta V_{RF} = R \cdot AMR \cdot \sin 2\varphi_H \cdot \cos\varphi_H \cdot I_{AC} \cdot I_{RF} \cdot \left(\beta_{FL}\chi_{xx}^{RF} + \beta_{DL}\chi_{xy}^{RF} + \beta_{FL}\chi^{AC}\right) \Big/ (w \cdot M_s), \quad (2)$$

where R is the resistance, AMR is the anisotropic magnetoresistance ratio. This RF voltage signal can be viewed as a result of current-induced impedance (CIZ),

$$\Delta Z = \frac{\Delta V_{RF}}{I_{RF}} = R \cdot AMR \cdot \sin 2\varphi_H \cdot \cos\varphi_H \cdot I_{AC} \cdot \left(\beta_{FL}\chi_{xx}^{RF} + \beta_{DL}\chi_{xy}^{RF} + \beta_{FL}\chi^{AC}\right) \Big/ (w \cdot M_s). \quad (3)$$

Here, we propose a CIZ-based ST-FMR (CIZ-ST-FMR) to determine β_{DL} and β_{FL} by measuring the RF reflection resulting from ΔZ. The setup of this CIZ-ST-FMR is sketched in Fig. 1, when switch S1 is closed and S2 is connected to terminal *a*. A vector network analyzer is used as the RF source, which is amplified by an RF amplifier. The RF power is subsequently split into two paths. The upper path is the reference RF signal, which goes through an isolator made of a circulator with a 50 Ω impedance terminal. The circulator is optimized around 5.8 GHz. A phase shifter allows control of the phase in the reference signal, which can be monitored by the vector network analyzer via a 10 dB directional coupler. The RF signal in the lower path is injected into the sample after passing through a circulator and a bias Tee. Simultaneously, an alternating current at 1.111 kHz frequency is applied to the sample through the bias Tee. The reflected RF signal is redirected to an RF mixer by the circulator, where it rectifies with the reference RF signal. The mixed signal, which contains both an AC and a DC component, undergoes further filtering using a low-pass filter with cut off frequency of 470 MHz. The AC component, namely the AC mixed voltage, is measured by a lock-in amplifier. The DC component, namely the DC mixed voltage, is detected by a voltmeter.

Since the anisotropic magnetoresistance change is usually much smaller than the original resistance, to the first-order approximation, the AC mixed voltage due to ΔZ can be expressed as

$$V_{mix\_AC} = Y \cdot \mathrm{Re}\left[\Delta Z \cdot e^{i(X - \Delta\Phi_{RF})}\right], \quad (4)$$

where Y is a constant related to the RF reflection coefficient of the device as well as the sensitivity of the mixer, X is the phase difference between the CIZ-related RF reflection and the reference RF signal, and $\Delta\Phi_{RF}$ is the additional phase change from the phase shifter.

We demonstrate the feasibility of the CIZ-ST-FMR with a//Py (=$Ni_{80}Fe_{20}$, 5)/Pt(3) magnetic bilayer, where "//" denotes the silicon substrate with thermal oxides, and the numbers in parenthesis are in nanometers. The samples are patterned into short stripes 5 μm in

width and 10 μm in length. The stripe is connected to a coplanar waveguide made of Ti(5)/Au(80) placed in the RF circuit shown in Fig. 1. The same system in Fig. 1 can be used to measure the conventional ST-FMR, when switch S1 is open and switch S2 is connected to terminal *b*. The rectified DC voltage from the conventional ST-FMR is shown in Fig. 2(a). Here, the RF frequency is 6 GHz, the nominal RF power is about 9 dBm, and the angle between the external magnetic field and RF current direction is $\varphi_H = 45°$, unless otherwise specified. The same RF parameters are kept when the setup is switched to the CIZ-ST-FMR. The AC mixed signal V_{mix_AC} measured by the lock-in amplifier is shown in Fig. 2(b). The signal-to-noise ratio is comparable to the conventional ST-FMR. As can be understood from Eqs. (3) and (4), V_{mix_AC} contains three components: the symmetric and antisymmetric Lorentzian components due to the ferromagnetic resonance susceptibility χ_{xx} and χ_{xy}, and a nearly $1/H_{ext}$-dependence due to χ_{AC}.

While the conventional ST-FMR signal is only due to the real part of magnetic susceptibilities, the CIZ-ST-FMR signal measures both real and imaginary parts of the susceptibilities. Due to the nature of RF mixing, the mixed signal in the CIZ-ST-FMR measurement is very sensitive to the RF phase. Since χ_{AC} is the low-frequency magnetic susceptibility, it shall have a negligible imaginary component. As suggested in Eq. (4), when the relative phase $X - \Delta\Phi_{RF}$ is 90°, the $1/H_{ext}$-dependence curve in V_{mix_AC} should vanish. This feature serves as a marker to aid in selecting the optimal $\Delta\Phi_{RF}$ for the phase shifter. We fit the CIZ-ST-FMR curve with the following equation:

$$V_{mix\_AC} = A\frac{\Delta H^2}{(H_{ext}-H_r)^2+\Delta H^2} + B\frac{\Delta H(H_{ext}-H_r)}{(H_{ext}-H_r)^2+\Delta H^2} + C\frac{1}{H+H_a} + D, \quad (5)$$

where H_r is the resonance field, ΔH is the resonance linewidth, H_a is the effective in-plane anisotropy field, which is very low for Py. Here, *A*, *B*, *C*, and *D* are coefficients for the symmetric Lorentzian resonance signal, antisymmetric Lorentzian resonance signal, AC susceptibility-induced signal, and constant offset, respectively.

By tuning the phase shifter, we find that when $\Delta\Phi_{RF} = 142°$, the parameter *C* for χ_{AC} is minimized, as seen in Fig. 2(c). Conversely, the parameter *C* maximizes when the phase is shifted 90° further, at $\Delta\Phi_{RF} = 52°$, as seen in Fig. 2(d). For data at $\Delta\Phi_{RF} = 142°$, fitting to the Lorentzian resonance shows that the ratio between the symmetric and antisymmetric component is $\frac{V_{mix}^{sym}}{V_{mix}^{asym}} = -1.94 \pm 0.02$. This ratio is equivalent to $\frac{\beta_{FL}}{\beta_{DL}}\frac{\mathrm{Im}[\chi_{xx}^{RF}]}{\mathrm{Im}[\chi_{xy}^{RF}]}$, as can be understood from Eq. (4). In the conventional ST-FMR experiment, from the data shown in Fig. 2(a), we extrapolate $\frac{V_{rectifying}^{sym}}{V_{rectifying}^{asym}} = 0.51 \pm 0.01$, which is equivalent to $\frac{\beta_{DL}}{\beta_{FL}}\frac{\mathrm{Re}[\chi_{xy}^{RF}]}{\mathrm{Re}[\chi_{xx}^{RF}]}$. The multiplication of the two ratios is very close to −1, suggesting quantitative agreement in the line shape analysis between the two techniques (see section 4 in the supplementary material for details).

The CIZ-ST-FMR measurement allows extrapolation of spin–orbit torques beyond the line shape analysis. For further analysis of the

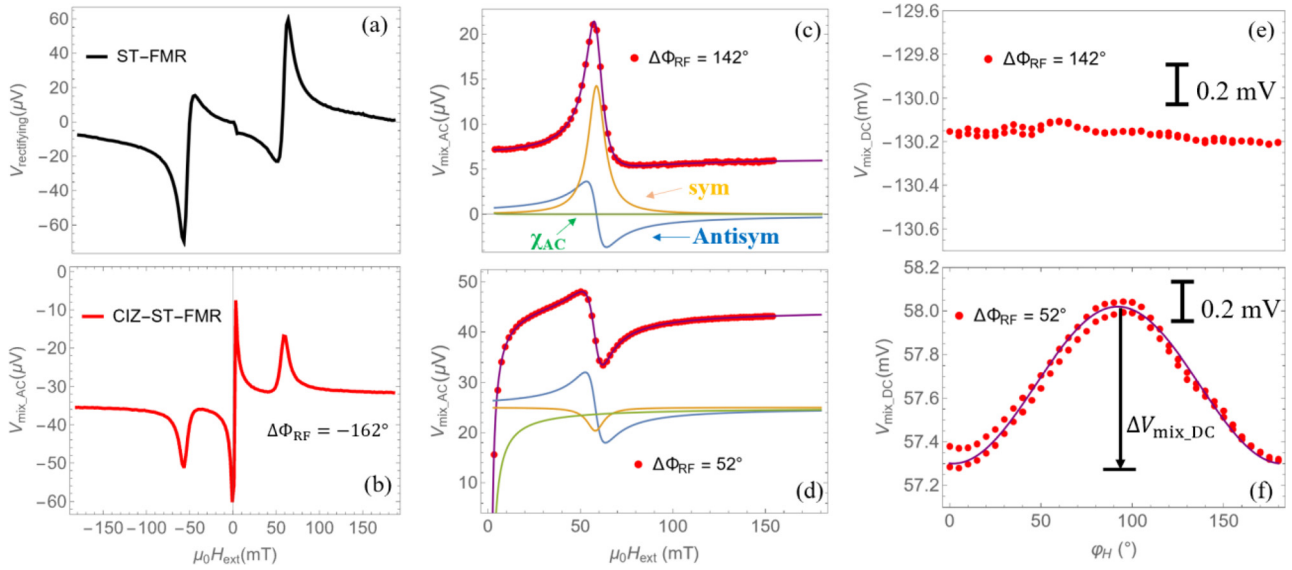

FIG. 2. (a) Measured ST-FMR signal of the Py/Pt bilayer sample by a nanovolt meter. The microwave frequency is at 6 GHz and $\varphi_H = 45°$. (b) CIZ-ST-FMR signal V_{mix_AC} measured under the same condition as the conventional ST-FMR measurement. The relative phase created by the phase shifter is $\Delta\Phi_{RF} = -162°$. (c) When the phase shift is tuned to $\Delta\Phi_{RF} = 142°$, the signal due to χ_{AC} is significantly suppressed, suggesting that at this phase the CIZ-ST-FMR signal is not sensitive to the real part of ΔZ. The red dots are experimental data. The purple line is the fitting to the signal according to Eq. (5), with the three components, respectively, plotted in orange (symmetric Lorentzian), blue (antisymmetric Lorentzian) and green colors (χ_{AC}). For clarity, the curves for the three components are vertically shifted. (d) When the phase shift is tuned to $\Delta\Phi_{RF} = 52°$ and 90° away from that in (c), the signal due to χ_{AC} is maximized, while that due to χ_{RF} is also altered. (e) and (f) For calibration, we measure the DC component of the mixing voltage, V_{mix_DC}, while rotating the external magnetic field kept at 14 mT from $\varphi_H = 0°$ to 180° and back to 0°. The φ_H-dependence is minimized at $\Delta\Phi_{RF} = 142°$, and maximized at $\Delta\Phi_{RF} = 52°$. The φ_H-dependence is fitted with a simple $\cos^2\varphi_H$-function [purple curve in (f)] according to Eq. (6). The peak-to-peak value is the AMR-induced change to the DC mixing voltage, ΔV_{mix_DC}.

CIZ-ST-FMR, we carry out a calibration measurement. By rotating the external magnetic field, the resistance of the device varies due to anisotropic magnetoresistance. The DC mixed voltage changes, similar to that of Eq. (4),

$$V_{\mathrm{mix\_DC}} = \Delta V_{\mathrm{mix\_DC}} + W(\Delta\Phi_{\mathrm{RF}}) = Y \cdot \mathrm{Re}\left[R \cdot AMR \cdot \cos^2\varphi_{\mathrm{H}} \cdot e^{i(X-\Delta\Phi_{\mathrm{RF}})}\right] + W(\Delta\Phi_{\mathrm{RF}}), \quad (6)$$

where $W(\Delta\Phi_{\mathrm{RF}})$ is a background voltage independent of AMR, and $\Delta V_{\mathrm{mix\_DC}}$ is the *AMR*-induced change in the DC mixed voltage. The φ_{H}-dependence of the DC mixed voltage is shown in Figs. 2(e) and 2(f). Since the impedance change due to the anisotropic magnetoresistance only has a real part, the $\cos^2\varphi_{\mathrm{H}}$-dependence maximizes at $\Delta\Phi_{\mathrm{RF}} = 52°$ and minimizes at $\Delta\Phi_{\mathrm{RF}} = 142°$, coinciding with the maximum and minimum of χ_{AC}-induced AC mixed signal as in Figs. 2(c) and 2(d). From the $\cos^2\varphi_{\mathrm{H}}$-dependence at $\Delta\Phi_{\mathrm{RF}} = 52°$, one can extrapolate that the coefficient $Y \cdot R \cdot AMR = -0.68 \pm 0.01$ mV. On the other hand, according to Eqs. (3) and (4), the AC mixed signal measured at $\Delta\Phi_{\mathrm{RF}} = 142°$, shown in Fig. 2(c), can be expressed as

$$V_{\mathrm{mix\_AC}} = \frac{1}{\sqrt{2}} Y \cdot R \cdot AMR \cdot I_{\mathrm{AC}} \cdot \left(\beta_{\mathrm{FL}}\mathrm{Im}[\chi_{xx}^{\mathrm{RF}}] + \beta_{\mathrm{DL}}\mathrm{Im}[\chi_{xy}^{\mathrm{RF}}]\right) \Big/ (w \cdot M_{\mathrm{s}}). \quad (7)$$

Using the magnetic susceptibility derived from the Landau–Lifshitz–Gilbert equation (see section 4 in the supplementary material), we extrapolate the $\beta_{\mathrm{FL}} = 0.343 \pm 0.008$ and $\beta_{\mathrm{DL}} = 0.679 \pm 0.014$. It is important to note that in Eq. (7), I_{AC} explicitly shows up, while I_{RF} is embedded in Y, which is measured experimentally.

As an independent check, we employed an alternative method for determining the damping-like and field-like spin torque by measuring the ST-FMR linewidth ΔH and resonant field H_{r} as a function of DC. The experimental results are shown in Fig. 3. The extrapolated damping-like and field-like torque coefficients are $\beta_{\mathrm{DL\_DC}} = 0.63 \pm 0.03$ and $\beta_{\mathrm{FL\_DC}} = 0.33 \pm 0.02$, consistent with those determined from the CIZ-ST-FMR technique, but with a much larger uncertainty (see section 5 in the supplementary material for details). We therefore believe that the CIZ-ST-FMR technique provides a more accurate method to independently measure the damping-like and field-like torques compared to its counterparts.

We also conducted a phase-dependence study by tuning the $\Delta\Phi_{\mathrm{RF}}$ from the phase shifter. For each phase, the field-dependent AC mixed voltage in the CIZ-ST-FMR experiment is measured by the lock-in amplifier, and the signal is fitted according to Eq. (5) to obtain coefficients *A*, *B*, and *C*. In addition, the field-angle-dependence of the DC mixed voltage is measured to show the impact from the AMR. As can be understood from Eqs. (3), (4), and (6), both χ_{AC} and *AMR* only influence the real part of the impedance. Therefore, they are in phase with each other, as seen in Figs. 4(a) and 4(b). Indicated in Fig. 4(c), the coefficients *A* and *B* due to symmetric and antisymmetric Lorentzian resonance in the AC mixed voltage are 90° shifted from each other, consistent with Eq. (3).

According to Eq. (2), the AC mixed signal is proportional to $I_{\mathrm{RF}}I_{\mathrm{AC}}$. To test this relationship, the magnitude of the alternating current is varied, with all other RF parameters kept the same. Shown in Fig. 4(d), the AC mixed voltage is indeed linear with the alternating current. The RF power-dependence is also carried out on the same sample. A coaxial variable attenuator is used to adjust the RF power, P_{RF}. The RF circuit is modified (see section 7 in the supplementary material for details) by moving the phase shifter to the lower path to compensate for the additional phase change from tuning the attenuator. Shown in Fig. 4(e), the AC mixed voltage measured in the CIZ-ST-FMR experiment is proportional to $\sqrt{P_{\mathrm{RF}}}$. As a comparison, the rectifying voltage measured in the conventional ST-FMR experiment is proportional to I_{RF}^2, hence proportional to P_{RF}.

As the CIZ-ST-FMR signal is proportional to the square root of RF power, it is free of complication from DC spin pumping-induced inverse spin Hall signal,[34–36] which is one of the spurious signals in the conventional ST-FMR measurement. However, the CIZ-ST-FMR may be subject to complications from Faraday effect-induced induction and AC spin pumping. Both effects generate an impedance in the device proportional to the magnetic susceptibility. Since the ferromagnetic resonance linewidth and resonance field can be modulated by an applied current, the CIZ-ST-FMR measurement may also pick up signals due to current-modulated magnetic susceptibility. We estimate the spurious signal to be at most 10% of the CIZ-ST-FMR signal (see section 9 in the supplementary material).

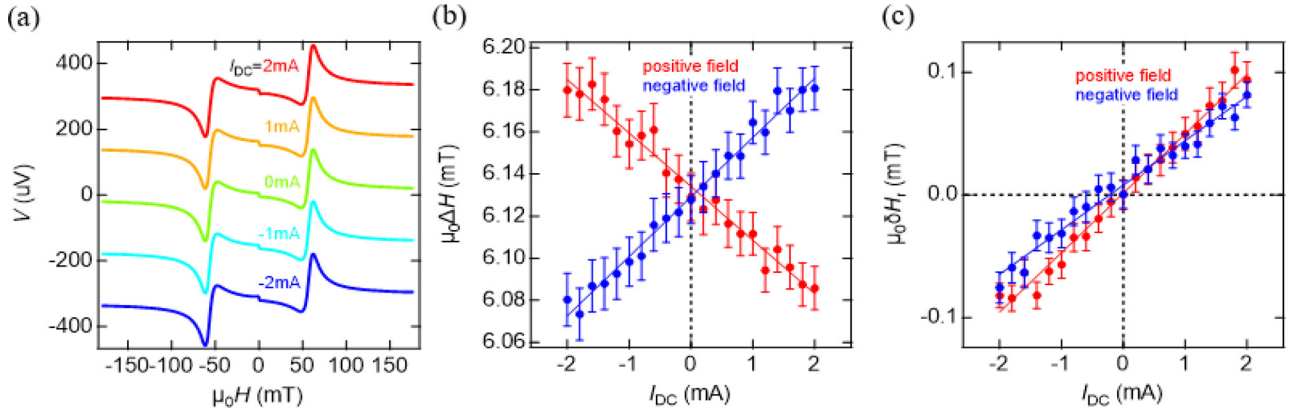

FIG. 3. (a) Measured DC-induced ST-FMR signal of the Py/Pt bilayer sample. The microwave frequency is at 6 GHz and $\varphi_H = 45°$. (b) and (c) Current-dependence of the FMR linewidth $\mu_0\Delta H$ (b) and resonant magnetic field change $\mu_0\delta H_r$ (c).

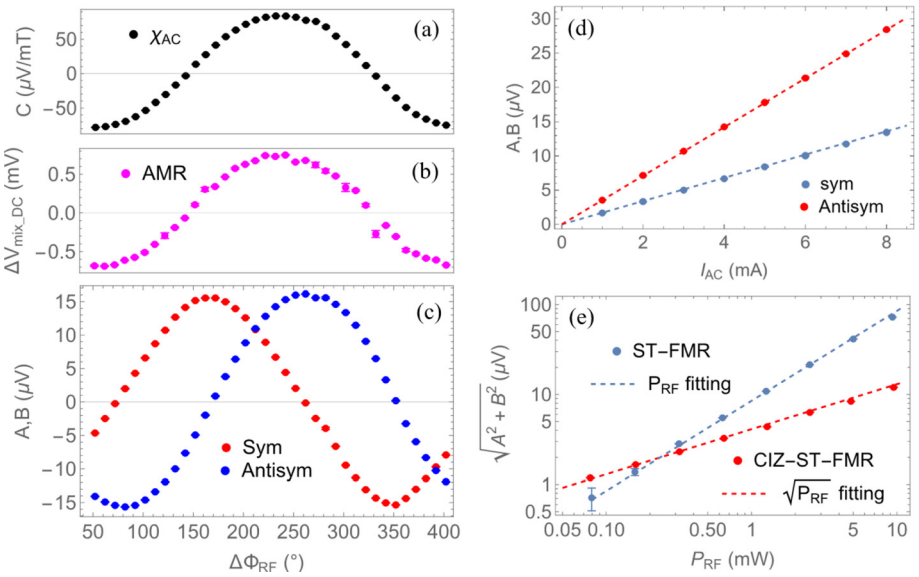

FIG. 4. (a)–(c) RF phase-dependence of the phase shifter on (a) the parameter C for χ_{AC}, (c) the parameter A for the symmetric Lorentzian component, the parameter B for the antisymmetric Lorentzian component based on fitting to Eq. (5) and (b) the AMR-induced DC mixed voltage signal ΔV_{mix_DC}. (d) I_{AC}-dependence of AC mixed voltage, where the additional phase from the phase shifter is chosen as $\Delta\Phi_{RF} = 232^\circ$. Dashed lines are linear fittings. (e) RF power-dependence of the AC mixed voltage in a log–log plot. Since ST-FMR and CIZ-ST-FMR may have different line shapes, e.g., one may have a dominantly symmetric Lorentzian line shape and the other may have a dominant antisymmetric line shape, $\sqrt{A^2+B^2}$ is plotted to compare the signal strengths between the two measurements.

In conclusion, we have demonstrated a modified ST-FMR technique based on current-induced impedance. The developed technique has comparable signal-to-noise ratio as the conventional ST-FMR. It also offers additional advantages over the conventional ST-FMR that the CIZ-ST-FMR allows independent extrapolation of the field-like torque and damping-like torque efficiencies, without the need to calibrate the RF current. These results are consistent with another type of ST-FMR that measures the current-induced linewidth broadening and peak position shift, but offer much lower uncertainty. It should be pointed out that there may be small but systematic artificial signals due to induction and AC spin pumping, which requires scrutinization to further improve the measurement accuracy. We suggest that the proposed CIZ-ST-FMR could be a powerful tool for measuring spin–orbit torques.

See the supplementary material for detailed derivations, information on dependences of power and magnetic field angle, as well as additional experimental parameters.

X.F. acknowledges support from the JSPS visiting fellowship, the DU FRF grant, and the NSF award (2047118). This work was also supported by the JSPS KAKENHI through Grant Nos. JP23KK0093, JP22H01936, JP22J12061, JP21H04562, and JP20H05665, the Iketani Science and Technology Foundation, Collaborative Research Program of the Institute for Chemical Research, Kyoto University. We would also like to thank Professor Bo Yang for help with RF components.

AUTHOR DECLARATIONS

Conflict of Interest

The authors have no conflicts to disclose.

Author Contributions

Yuta Kobayashi: Data curation (lead); Formal analysis (equal); Funding acquisition (supporting); Investigation (lead); Writing – original draft (equal); Writing – review & editing (lead). **Tomoya Itoh:** Investigation (equal). **Ryusuke Hisatomi:** Investigation (equal); Methodology (equal); Supervision (equal); Writing – review & editing (equal). **Takahiro Moriyama:** Funding acquisition (equal); Resources (equal); Supervision (equal); Writing – review & editing (equal). **Yoichi Shiota:** Conceptualization (equal); Funding acquisition (equal); Investigation (equal); Resources (lead); Software (lead); Supervision (equal); Writing – review & editing (equal). **Xin Fan:** Conceptualization (lead); Data curation (equal); Formal analysis (equal); Funding acquisition (equal); Investigation (equal); Methodology (lead); Project administration (lead); Supervision (lead); Visualization (lead); Writing – original draft (lead); Writing – review & editing (equal). **Teruo Ono:** Funding acquisition (equal); Resources (equal); Supervision (equal); Writing – review & editing (supporting).

DATA AVAILABILITY

The data that support the findings of this study are available from the corresponding authors upon reasonable request.

REFERENCES

[1]A. Manchon, J. Železný, I. M. Miron, T. Jungwirth, J. Sinova, A. Thiaville, K. Garello, and P. Gambardella, Rev. Mod. Phys. **91**, 035004 (2019).
[2]I. M. Miron, K. Garello, G. Gaudin, P. J. Zermatten, M. V. Costache, S. Auffret, S. Bandiera, B. Rodmacq, A. Schuhl, and P. Gambardella, Nature **476**, 189–193 (2011).
[3]L. Liu, C. F. Pai, Y. Li, H. W. Tseng, D. C. Ralph, and R. A. Buhrman, Science **336**, 555–558 (2012).
[4]A. M. Humphries, T. Wang, E. R. J. Edwards, S. R. Allen, J. M. Shaw, H. T. Nembach, J. Q. Xiao, T. J. Silva, and X. Fan, Nat. Commun. **8**, 911 (2017).
[5]L. Liu, T. Moriyama, D. C. Ralph, and R. A. Buhrman, Phys. Rev. Lett. **106**, 036601 (2011).
[6]M. Harder, Z. X. Cao, Y. S. Gui, X. L. Fan, and C.-M. Hu, Phys. Rev. B **84**, 054423 (2011).
[7]D. Lee, D. Go, H.-J. Park, W. Jeong, H.-W. Ko, D. Yun, D. Jo, S. Lee, G. Go, J. H. Oh, K.-J. Kim, B.-G. Park, B.-C. Min, H. C. Koo, H.-W. Lee, O. Lee, and K.-J. Lee, Nat. Commun. **12**, 6710 (2021).

[8]R. Fukunaga, S. Haku, H. Hayashi, and K. Ando, Phys. Rev. Res. **5**, 023054 (2023).
[9]C.-F. Pai, L. Liu, Y. Li, H. W. Tseng, D. C. Ralph, and R. A. Buhrman, Appl. Phys. Lett. **101**, 122404 (2012).
[10]A. R. Mellnik, J. S. Lee, A. Richardella, J. L. Grab, P. J. Mintun, M. H. Fischer, A. Vaezi, A. Manchon, E.-A. Kim, N. Samarth, and D. C. Ralph, Nature **511**, 449–451 (2014).
[11]T. Moriyama, S. Takei, M. Nagata, Y. Yoshimura, N. Matsuzaki, T. Terashima, Y. Tserkovnyak, and T. Ono, Appl. Phys. Lett. **106**, 162406 (2015).
[12]W. Zhang, M. B. Jungfleisch, F. Freimuth, W. Jiang, J. Sklenar, J. E. Pearson, J. B. Ketterson, Y. Mokrousov, and A. Hoffmann, Phys. Rev. B **92**, 144405 (2015).
[13]Y. Ou, S. Shi, D. C. Ralph, and R. A. Buhrman, Phys. Rev. B **93**, 220405(R) (2016).
[14]K. Kondou, R. Yoshimi, A. Tsukazaki, Y. Fukuma, J. Matsuno, K. S. Takahashi, M. Kawasaki, Y. Tokura, and Y. Otani, Nat. Phys. **12**, 1027–1031 (2016).
[15]W. Zhang, W. Han, S.-H. Yang, Y. Sun, Y. Zhang, B. Yan, and S. S. P. Parkin, Sci. Adv. **2**, e1600759 (2016).
[16]H. An, Y. Kageyama, Y. Kanno, N. Enishi, and K. Ando, Nat. Commun. **7**, 13069 (2016).
[17]D. MacNeill, G. M. Stiehl, M. H. D. Guimaraes, R. A. Buhrman, J. Park, and D. C. Ralph, Nat. Phys. **13**, 300–305 (2017).
[18]Z. Xu, G. D. H. Wong, J. Tang, E. Liu, W. Gan, F. Xu, and W. S. Lew, ACS Appl. Mater. Interfaces **12**(29), 32898–32904 (2020).
[19]Y. Hibino, T. Taniguchi, K. Yakushiji, A. Fukushima, H. Kubota, and S. Yuasa, Nat. Commun. **12**, 6254 (2021).
[20]K. Kondou, H. Chen, T. Tomita, M. Ikhlas, T. Higo, A. H. MacDonald, S. Nakatsuji, and Y. Otani, Nat. Commun. **12**, 6491 (2021).
[21]P. Wang, A. Migliorini, S.-H. Yang, J.-C. Jeon, I. Kostanovskiy, H. Meyerheim, H. Han, H. Deniz, and S. S. P. Parkin, Adv. Mater. **34**, 2109406 (2022).
[22]L. Yu, S. Karube, M. Liu, M. Tsunoda, M. Oogane, and Y. Ando, Appl. Phys. Express **15**, 033002 (2022).
[23]H. Bai, L. Han, X. Y. Feng, Y. J. Zhou, R. X. Su, Q. Wang, L. Y. Liao, W. X. Zhu, X. Z. Chen, F. Pan, X. L. Fan, and C. Song, Phys. Rev. Lett. **128**, 197202 (2022).
[24]S. Karube, T. Tanaka, D. Sugawara, N. Kadoguchi, M. Kohda, and J. Nitta, Phys. Rev. Lett. **129**, 137201 (2022).
[25]C.-F. Pai, Y. Ou, L. H. Vilela-Leão, D. C. Ralph, and R. A. Buhrman, Phys. Rev. B **92**, 064426 (2015).
[26]M.-H. Nguyen and C.-F. Pai, APL Mater. **9**, 030902 (2021).
[27]T. Ikebuchi, Y. Shiota, T. Ono, K. Nakamura, and T. Moriyama, Appl. Phys. Lett. **120**, 072406 (2022).
[28]X. Fan, J. Wu, Y. Chen, M. J. Jerry, H. Zhang, and J. Q. Xiao, Nat. Commun. **4**, 1799 (2013).
[29]J. Kim, J. Sinha, M. Hayashi, M. Yamanouchi, S. Fukami, T. Suzuki, S. Mitani, and H. Ohno, Nat. Mater. **12**, 240–245 (2013).
[30]K. Garello, I. M. Miron, C. O. Avci, F. Freimuth, Y. Mokrousov, S. Blügel, S. Auffret, O. Boulle, G. Gaudin, and P. Gambardella, Nat. Nanotechnol. **8**, 587–593 (2013).
[31]X. Fan, H. Celik, J. Wu, C. Ni, K.-J. Lee, V. O. Lorenz, and J. Q. Xiao, Nat. Commun. **5**, 3042 (2014). (2014).
[32]B. Han, B. Zhang, S. Sun, B. Wang, Y. Guo, and J. Cao, J. Appl. Phys. **130**, 213902 (2021).
[33]X. Fan, A. R. Mellnik, W. Wang, N. Reynolds, T. Wang, H. Celik, V. O. Lorenz, D. C. Ralph, and J. Q. Xiao, Appl. Phys. Lett. **109**, 122406 (2016).
[34]K. Kondou, H. Sukegawa, S. Kasai, S. Mitani, Y. Niimi, and Y. Otani, Appl. Phys. Express **9**, 023002 (2016).
[35]A. Okada, Y. Takeuchi, K. Furuya, C. Zhang, H. Sato, S. Fukami, and H. Ohno, "Spin-pumping-free determination of spin-orbit torque efficiency from spin-torque ferromagnetic resonance," Phys. Rev. Appl. **12**, 014040 (2019).
[36]A. Kumar, S. Akansel, H. Stopfel, M. Fazlali, J. Åkerman, R. Brucas, and P. Svedlindh, "Spin transfer torque ferromagnetic resonance induced spin pumping in the Fe/Pd bilayer system," Phys. Rev. B **95**, 064406 (2017).